Supporting Information

Dual-electron enhanced effect in K- doped MoS$_2$ few layers for

high electrocatalytic activity as the counter electrode in

dye-sensitized solar cells

Yuna Yan[1], Gang Shen[1], Rui Song[2†] and Kunquan Hong[1]*

[1]School of Physics, Southeast University, Nanjing, 211189, China
Email: hongkq@gmail.com;

[2]Department of General Education, Army Engineering University
of People's Liberation Army, Nanjing 211101, China

Email: snoopysr@163.com

Experimental section

Sample preparation:

In the chemical vapour deposition (CVD) method, after the FTO glass was cleaned carefully and dried in Ar flow, 1 mol/L KOH solution is spin coated on this clean FTO substrate at first. Then a layer of Mo precursors were deposited by spin coating a 0.005mol/L ammonium molybdate solution. The FTO glass after KOH treatment and Mo precursor deposition is placed in the center of the quartz tube of a tube furnace. 2g sulfur powder is placed at the upstream of the FTO glass. Then argon gas (99.999%) with a flow rate of 30 sccm (cubic centimetres per minute at STP) was introduced the quartz tube and the pressure was maintained at 30 mbar. The center of the quartz tube was heated to 450 °C and this temperature was kept for 20min. The temperature of the sulfur powder

was raised to 200 °C simultaneously. When the temperature decreases to room temperature naturally, the samples were taken out for measurements. Pure MoS_2 was synthesizes by the same procedures and condition except without KOH treatment.

In the pulsed laser deposition (PLD) method: 1 mol/L KOH solution is spin coated on this clean FTO substrate at first. Then a MoS_2 target was sputtered by using a KrF excimer laser in the pulsed laser deposition system. The laser energy is set to 200mJ/pulse with 500 pulses. A thin layer of MoS_2 film can be obtained at room temperature. Pure MoS_2 was synthesized by the same procedures and condition except the FTO glass without KOH treatment.

Characterization:

The morphology, microstructure and properties of the samples were characterized by scanning electron microscope (FESEM, FEI inspect F50), transmission electron microscope (TECNAI G2 F20) and confocal Raman system (Horiba jobin). X-ray photoelectron spectroscopy (XPS, Thermo Fischer, ESCALAB 250 Xi) was used to analyse the elemental composition of the sample. The photocurrent density-voltage characteristic curves (J-V) are tested under AM 1.5 G (1000W/m^2) simulated sunlight using a solar simulator. These thin films are used as the counter electrodes. TiO_2 film prepared by a screen-printing method is used as the photoanode. The thickness of the TiO_2 film is about 5.5 μm. Before solar cell assembling, this photoanode was annealed again in air at 450 °C for 30 minutes. After the sample was cooled naturally to 80 °C, it was immersed into dye solution of 0.5 mM $(Bu_4N)_2[Ru(4,4'-(COOH)-2,2,-bipyridine)_2 (NCS)_2]$ (N719 dye) in ethanol for 12 h. Then the photoanode was washed with ethanol twice and dried in N_2 flow. The sandwich solar cell structure with photoanode, electrolyte and counter electrode were assembled with the area of 25 mm^2. The electrolyte (composed of iodine, anhydrous lithium iodide, PMII, guanidine isothiocyanate, TBP, and acetonitrile) was introduced into the gap formed by the two electrodes by capillary

force. To measure the electrochemical impedance spectroscopy (EIS), two identical substrates were assembled together and tested by an electrochemical workstation (CHI760D). The area of electrodes is 1cm^2. The electrolyte used in EIS measurement is an acetonitrile solution of 10 mM LiI, 1 mM I_2, and 0.1 M $LiClO_4$.

Theoretical calculations:

First-principles calculations were performed based on the density functional theory, using the Vienna *ab initio* simulation package (VASP)[1] with projected augmented wave (PAW) pseudopotentials. The Perdew−Burke−Ernzerhof functional and the generalized gradient approximation (GGA-PBE) were employed to describe the exchange−correlation interaction[2]. For all calculations, an energy cutoff of 500 eV was adopted for the plane wave basis expansion. Brillouin-zone integrations were performed based on the Γ-centered Monkhorst−Pack k-mesh, with the sampling density varying with lattice constants to ensure the desired accuracy. Atomic structures were fully relaxed until the Hellmann-Feynman forces were less than 0.01 eV/Å. The energy convergence criterion was set to 10^{-5} eV for both structural optimization and static calculation.
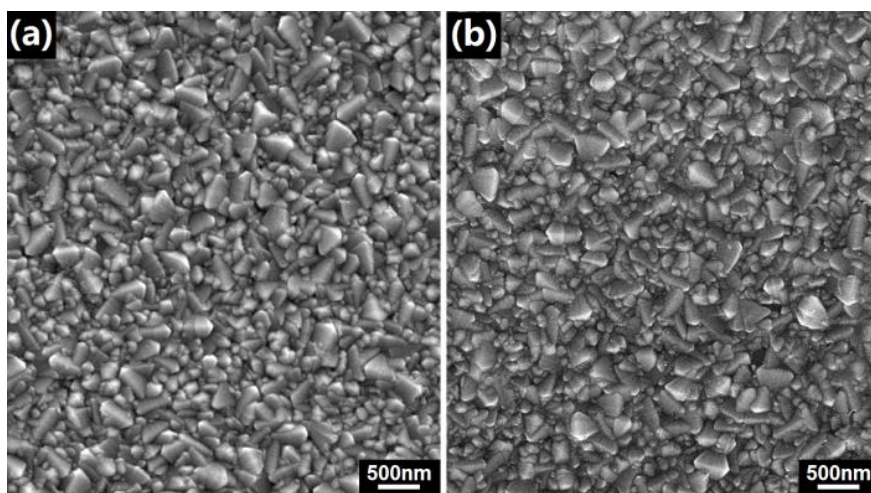
Figure S1. SEM images of pure FTO (a) and K-doped few layer MoS_2 on FTO (b).

Fig. S1 is the SEM image of pure clean FTO glass (Fig.S1a) and FTO substrate with MoS_2 film. Compared with the uniform brightness of the FTO surface (Fig.S1a), the K-doped MoS_2 thin film sample surface (Fig.1b) shows a different light and dark distribution, in which these parts presenting darker regions represent the presence of the MoS_2 films. Meanwhile, the outline of the FTO conductive glass substrate is still clearly visible in Fig. S1b, indicating that the thin MoS_2 film on the substrate is in thickness of fewer layers.
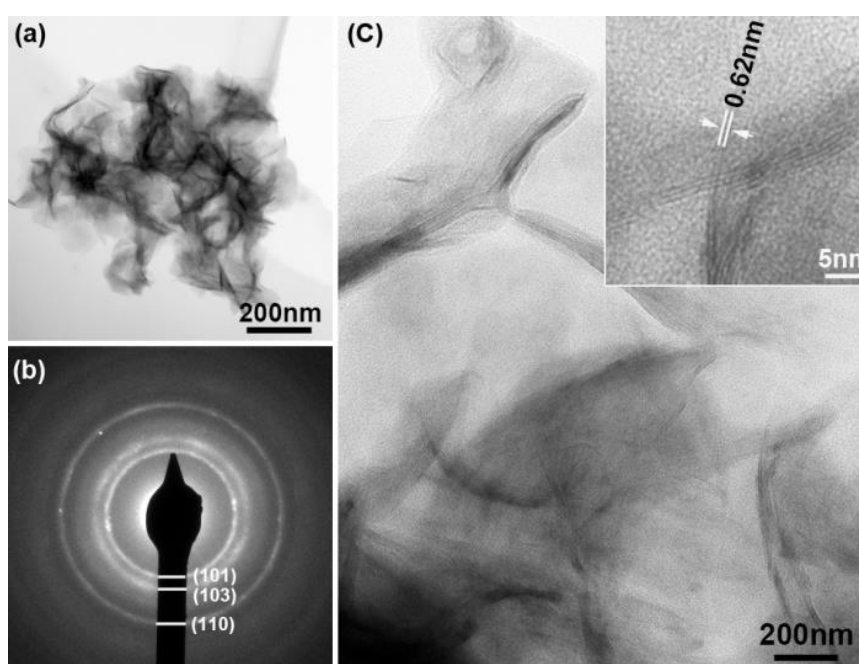
Figure S2. TEM image (a), SAED pattern (b) and HRTEM image of the few layer MoS_2 (c), in which it is pure MoS_2 with 2-4 layers.

The sample was further analysed by transmission electron microscope (TEM). As shown in Fig. S2, the TEM image shows that there is MoS_2 thin film grown on the FTO surface. The film thickness can be further determined by the high-resolution image (Fig. S2c), which is about 2-4 layers. The measured interlayer spacing is 0.62 nm (inset of Fig. S2c), which is consistent with the reported value of MoS_2. Moreover, three diffraction rings can be clearly seen in the selected area electron diffraction (SAED) pattern, corresponding to (101), (103) and (110) crystal planes of MoS_2, respectively (Fig. S2b).
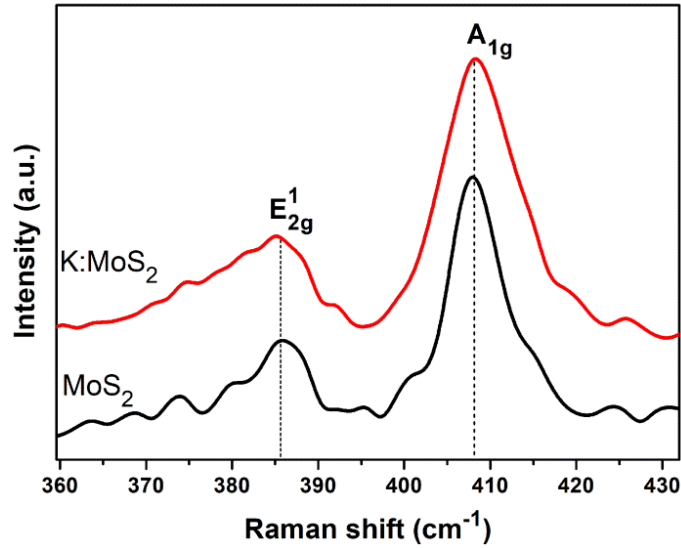
Figure S3. Raman spectra of K-MoS$_2$ film and MoS$_2$ film

The lattice vibration and Raman scattering properties of pure MoS$_2$ and K-MoS$_2$ samples was performed by a confocal Raman system. As shown in Fig. S3, the two characteristic peaks of the 2H phase MoS$_2$ are located at 386 and 408.5cm^{-1}, respectively, corresponding to two vibrational modes o E_{2g}^1 and A_{1g}. The vibration mode peak difference is 22.5cm^{-1}, which positively corresponds to the reported value of MoS$_2$ below 5 layers. The strong Raman peaks represents better crystallinity and lower defect of these MoS$_2$ film. The similar peak difference indicates pure MoS$_2$ and K-MoS$_2$ have almost the same thickness.

CEs	V_{oc}[V]	J_{sc}[mAcm^{-2}]	FF[%]	PCE[%]
Pt	0.747	11.6	73.1	6.34
MoS$_2$-CVD	0.764	11.4	62.8	5.47
K-MoS$_2$-CVD	0.784	12.8	67.4	6.76
MoS$_2$-PLD	0.724	11.15	71.1	5.74
K-MoS$_2$-PLD	0.733	12.4	72.5	6.56

Table S1. Photovoltaic parameters of the DSSCs base on Pt and MoS$_2$ and K-MoS$_2$ counter electrodes synthesized by CVD and PLD method.
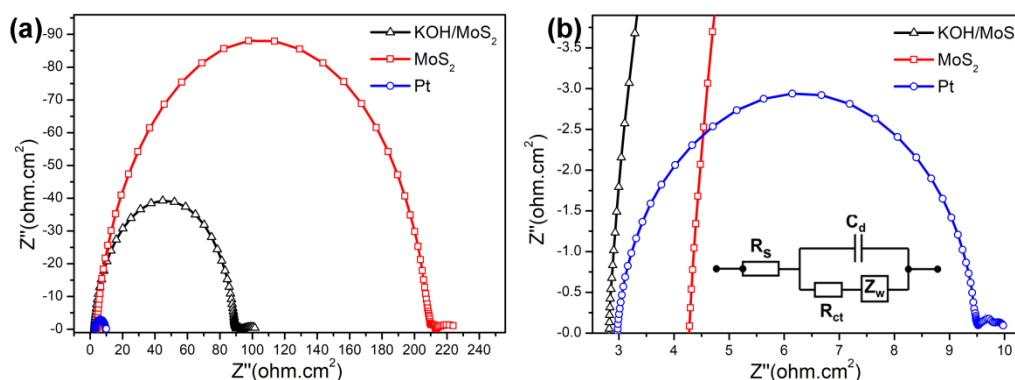
Figure S4. Electrochemical impedance spectroscopy (EIS) and the equivalent circuit of the of the symmetric cells with two identical counter electrodes of K-MoS$_2$, MoS$_2$ and Pt

The sample was characterized by electrochemical impedance spectroscopy as shown in Fig. S4. To extract the information from the EIS data, a suitable equivalent circuit model was established as the inset of Fig. S4b. The high frequency region intercept of the real axis represents the series resistance (R_s) term, the high frequency half-arc diameter represents the charge transfer resistance (R_{ct}) of electrons in the CEs. R_{ct} is associated to electron transfer reactions, such as catalysis of electron holes and metal sulfide surface sites. The EIS shows K-MoS$_2$, MoS$_2$ and Pt CEs have R_{ct} of 89.03, 209.4 and 9.50 ohm.cm^2, while the R_s is 2.83, 4.28 and 2.97 ohm.cm^2, respectively. These indicate the K-MoS$_2$ CE has smaller R_{ct} and R_s than those of the pure MoS$_2$ CE. So it can be seen those K-MoS$_2$ CEs shows obvious advantages than pure MoS$_2$. Besides, the R_s of K-MoS$_2$ CE is even a little smaller than that of the referenced Pt counter electrode. These indicate K atoms between FTO and MoS$_2$ play an important role to improve the photoelectric activity.
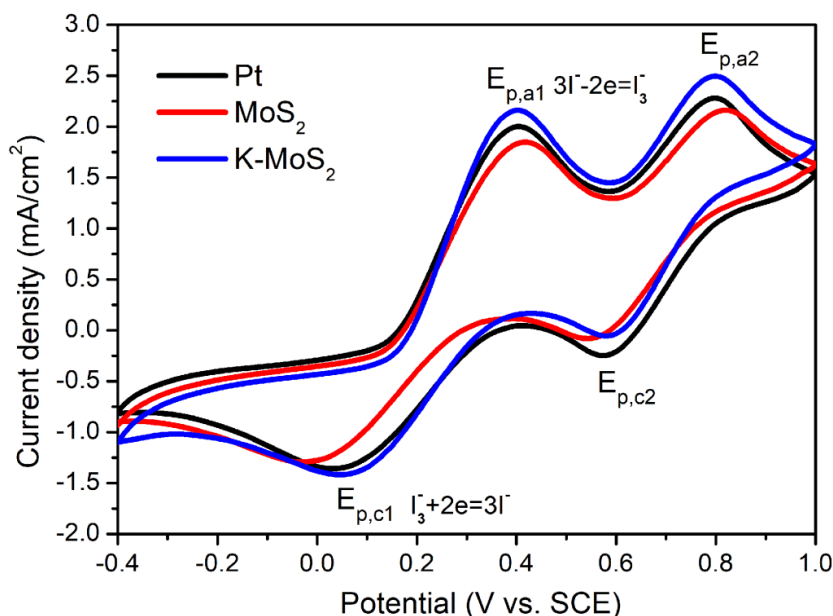
Figure S5.　Cyclic voltammetry (CV) plots of K-MoS$_2$, MoS$_2$ and Pt CEs.

Cyclic voltammetry (CV) was performed in a three-electrode system with a platinum sheet as counter electrode and an Ag/AgCl electrode as reference electrode. The prepared samples were used as the working electrodes. The electrolytes used for the test were 10 mM lithium iodide (LiI), 1 mM iodine (I$_2$) and 0.1 M lithium perchlorate (LiClO$_4$) in acetonitrile. The scanning range was -0.4 V to 1.0 V with the scanning rate is 50 mV/s. From the CV plots (Fig. S5), there are two pairs of redox peaks which correspond to two redox reactions. The redox peaks of $E_{p,c1}$ and $E_{p,a1}$ correspond to reaction of I$_3^-$ + 2e$^-$ ↔ 3I$^-$. The current density of the peaks and peak-to-peak potential difference (E_{pp}) in the plots can be compared to the catalytic activity of the material. The higher current density of the peaks indicates the higher catalytic activity of the material while the E_{pp} value is inversely related to the electrocatalytic performance. For the CV plots, the current density of the peaks is in order of J(K-MoS$_2$)>J(Pt)>J(MoS$_2$), indicating the K-MoS$_2$ has higher catalytic activity. Meanwhile, the E_{pp} value of K-MoS$_2$ is 355mV, which is slightly smaller than that of Pt (373mV) but significantly larger than that of pure MoS$_2$ (439mV). This result indicates that the two-electron effect in K-MoS$_2$ promotes the reduction of I$_3^-$ on the electrode surface, which in turn improves the electrocatalytic performance.
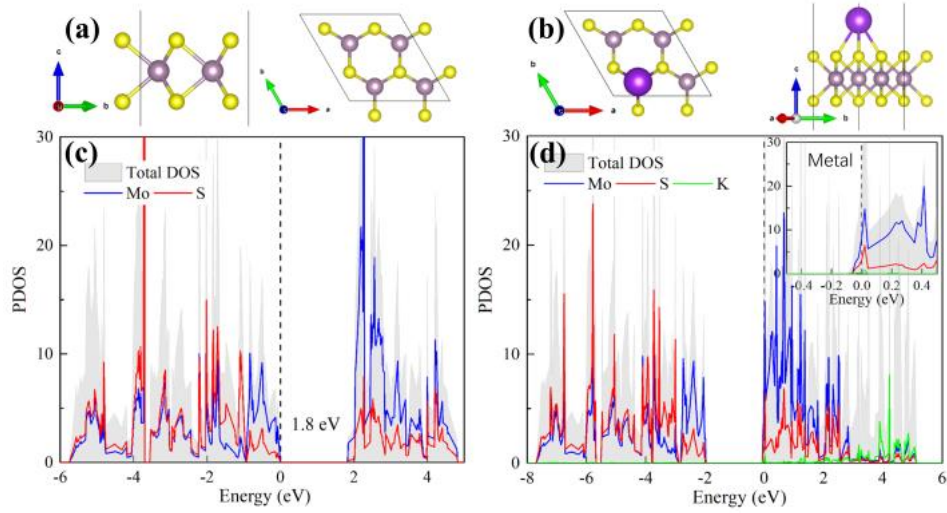
Figure S6. Top and side views of the optimized structures of MoS_2 (a) and K-MoS_2 (b). The density of state spectra was shown in (c) and (d) respectively.

References

1. G. Kresse and J. Furthmuller, *Phys. Rev. B*, 1996, **54**, 11169-11186.

2. J. P. Perdew, K. Burke and M. Ernzerhof, *Phys. Rev. Lett.*, 1996, **77**, 3865-3868.